Received: 24 December 2020 | Revised: 23 July 2021 | Accepted: 9 August 2021

DOI: 10.1002/ima.22651

RESEARCH ARTICLE

WILEY

Deep learning on compressed sensing measurements in pneumonia detection

Sheikh Rafiul Islam[1] | **Santi P. Maity**[1] | **Ajoy Kumar Ray**[2] | **Mrinal Mandal**[3]

[1]Department of Information Technology, Indian Institute of Engineering Science and Technology, Shibpur, India

[2]Centre for Data Science, JIS Institute of Advanced Studies and Research, Bidhannagar, India

[3]Department of Electrical & Computer Engineering, University of Alberta, Edmonton, Canada

Correspondence
Santi P. Maity, Department of Information Technology, Indian Institute of Engineering Science and Technology, Shibpur, India 711103.
Email: santipmaity@it.iiests.ac.in

Abstract

Pneumonia is one of the very common life-threatening diseases and needs proper diagnosis at an early stage to be cured expeditiously. Medical practitioners use chest X-ray as the best imaging modality to identify pneumonia. Due to the limited facilities available at the remote places and the need of maintaining the social distancing imposed by the recent outbreak of coronavirus disease, one may not have ease of access to a professional radiologist. This article proposes a deep learning (DL) framework that detects pneumonia from X-ray images to assist the medical practitioners located at distant places. The X-ray images are captured as compressed sensing (CS) measurements i.e. very few numbers of samples are observed in order to obtain an energy efficient and bandwidth preserving system to be utilized for far-end pneumonia detection purpose. Extensive simulation results show that the proposed approach enables the detection of pneumonia with 96.48% accuracy when only 30% samples are transmitted.

KEYWORDS

autoencoder, CNN, compressed sensing, deep learning, pneumonia detection

1 | INTRODUCTION

With the scarcity of medical facilities and support in hospital during this coronavirus disease (COVID-19) pandemic, tele-healthcare looks promising mode for providing care to the patients suffering from any type of illness that requires no surgery. Remote healthcare support not only facilitates medical treatment to the large section of the rural people but also reduces the burden of large number of patients from admission to the hospital, particularly during such pandemic situation. Tools and technologies involving tele-healthcare support may have a permanent impact even the COVID-19 ends as several statements made by the medical researchers are observed in the recent times. It is extremely necessary to provide the health services to the patients at remote locations suffering from the infectious diseases, to prevent the spreading of the disease by avoiding any kind of public exposure as well as for the sake of patients' own safety.

Pneumonia is often found to be one of the very common infectious diseases caused by bacteria, fungi, or viruses.[1] In severe cases, it leads to death, especially for the older adults, children of less than 5 years age and the people with other diseases or with an impaired immune system. Every year, around 1 (one) million people are detected with pneumonia, and around 50 000 die from the disease even in a developed country like the United States (U.S.) alone.[2] Medical practitioners use chest X-ray as the best imaging modality to diagnose pneumonia. However, a radiologist with rich domain expertise and experience is required for the proper analysis of the X-ray images. According to a study conducted by the World Health Organization (WHO), approximately two-thirds of the total population in the world do

not yet have access to a radiologist for the proper diagnosis of their diseases.

It would be of immense benefit if an automated computerized system is developed to analyze the X-ray images for appropriate diagnosis of the diseases. To offer proper medical services in remote locations, often imaging is performed at one end (by not so qualified operators) and interpretation/analysis needs to be performed by the medical practitioners at some far end. This requires the transmission of images over a communication medium or channel at low costs. Due to the low infrastructural cost as well as offering the facility of moderate and the long-distance coverage, wireless transmission channels are preferred to the wired medium. However, connection reliability, coverage range, data bandwidth support, and transmission energy requirement are the important issues in wireless transmission. To utilize and adapt the limited bandwidth of the wireless channel (as a large portion of spectrum occupied for several services), far-end image reconstruction to be accomplished from the subsample measurements of the images, which not only requires low bandwidth but also consumes low energy.[3] Compressive sensing (CS) enables signal reconstruction from the subsample measurements that are obtained at much lower sensing (sampling) rate than the actual requirement dictated by Shannon–Nyquist sampling theorem.[4,5] This leads to an energy and bandwidth efficient data transmission at the exchange of computation at the receiver. Such a signal processing approach not only offers a significant reduction in transmission bandwidth and energy requirement, but also reduces risks by enabling the reduction of harmful radiation from the X-ray imaging system as subsample data acquisition reduces the exposure time.[6,7]

Deep learning (DL), an artificial neural network (ANN) with a number of hidden layers, enables the extraction of hierarchical features from a given dataset directly, in order to perform on the real-world complex tasks.[8] Many times, the DL-based computer vision applications perform superior to human beings on recognition/detection tasks in terms of accuracy. Recently, the DL techniques have been used widely for analyzing biomedical images and extracting the useful insights from the images to be used for diagnosis purposes.[9–17] The possible applications of the DL techniques in conjunction with CS, in the field of biomedical radiology, are found to be more promising if it is extended for teleradiology systems. In this article, we propose a DL framework integrated with CS for the telediagnosis of pneumonia on the chest X-ray images. The utilization of CS leads to the significant reduction in the number of samples to be observed, which in turn reduces the transmission burden and energy. The proposed method enables the detection of pneumonia directly from the CS measurements observed at the remote end. The method also provides the reconstruction of the full-scale X-ray image, which in turn enables the medical practitioner to validate the detection result manually.

The remainder of the study is organized as follows: Section 2 presents a brief review on the state-of-the-art methods and scope of this work. The proposed pneumonia detection and X-ray image reconstruction framework are described in Section 3. The simulation results and discussion on the performance of the proposed method are presented in Section 4 and Section 5, respectively. Finally, Section 6 presents conclusions and future scopes of the work.

2 | LITERATURE REVIEW AND SCOPE OF THE PRESENT WORK

This section presents a brief review on the related state-of-the-art works and also states the scope and the contributions of this work.

2.1 | Literature review

Over the past decade, several learning-based methods utilizing natural language processing (NLP)[18–20] and DL[9–17] are studied to identify the different types of pneumonia. Fiszman et al.[18] used an automatic NLP tool to identify the acute bacterial pneumonia disease from the reports of the chest X-rays images. Chapman et al.[19] demonstrated a rule base, a probabilistic Bayesian network, and decision tree-based computerized methods to diagnose acute bacterial pneumonia from the chest X-ray reports. The performance of these resource-intensive applications are very much comparable to the human expertise. Mendonca et al.[20] proposed another NLP-based monitoring system for caring neonates to extract pneumonia-associated information from X-ray reports. However, these methods are very much dependent on the information provided by the X-ray reports and may lead to the inaccurate results if the reports are erroneous. Rajpurkar et al.[9] propose ChexNet that identifies pneumonia from the chest X-ray images directly, instead of relying on the reports. This method also helps to locate the infected areas by highlighting them through a heatmap. The approach uses DenseNet-121,[21] a pretrained 121 layer deep convolutional neural network (CNN), and applies transfer learning technique using the chest X-ray images to adapt the pretrained network for detecting pneumonia. Kermany et al.[10] developed a DL-based diagnostic tool utilizing transfer learning (TL) technique to adopt the

Inception-V3[22] network for identifying different treatable diseases. The tool demonstrates its capabilities by identifying blinding retinal diseases as well as pneumonia in chest X-ray images.

Jain et al.[11] proposed a customized DL model utilizing CNN for pneumonia detection from the chest X-ray images. Simulation results show that the customized model outperforms several existing models, namely, VGG-16,[23] ResNet-50,[24] and Inception-V3[22] adopted through TL. Togacar et al.[12] developed a DL framework that uses combined features obtained from the pretrained DL models comprising the AlexNet[25] and the VGG-16.[23] Every DL model extracts 1000 number of features and then gets reduced to total 300 combined features on the basis of redundancy and relevance. The extracted features are combined and used in a linear discriminant analysis (LDA) classifier to detect pneumonia. However, the model suffers from the overfitting problem, which leads to a low F1-score. The overfitting problem can be avoided by utilizing a residual structure in the customized CNN model as reported in Reference 13. The simulation results show that the approach helps to achieve a competitive F1-score along with the accuracy. In Reference 14, a DL model employing a pretrained Inception-V3[22] model as a feature extractor followed by a classifier is proposed for pneumonia detection from X-ray images. The simulation results show that the proposed approach achieves the maximum accuracy when support vector machine (SVM) is used as a classifier. Chouhan et al.[15] reported a DL framework employed on an ensemble method for the detection of pneumonia. This approach utilizes different neural networks pretrained on ImageNet as the feature extractors. The extracted features are then combined and fed to a classifier for the detection purpose. The simulation results show that the ensemble method outperforms the individual model for pneumonia detection. Yu et al.[16] reported another DL framework that uses a graph-knowledge embedded CNN to detect pneumonia from the X-ray images. The approach uses a pretrained model for the purpose of feature extraction. The extracted features are then combined using the graph to reconstruct a set of optimal features. Finally, a shallow one-layered neural network is utilized to classify the chest X-ray images as normal and pneumonia from the combined features.

In Reference 30, a denoising-based approximate message passing (D-AMP) CS reconstruction algorithm is proposed to recover the original sparse signal by imposing priors to the reconstruction process. However, the algorithm requires high computational resource and imposes practicality issue in resource-constrained far-end communication. Mousavi et al.[26] proposed a deep convolutional network (DCN) that enables reconstruction at 100 times faster speed than the conventional CS methods, while maintaining the desired quality. In Reference 31, an ANN is used to learn CS reconstruction inspired by D-AMP to reduce the computation complexity. In Reference 27, a DL model based on a conditional generative adversarial network (GAN) is used to reconstruct a magnetic resonance image (MRI) from CS measurements. The method reduces aliasing artifacts in the reconstructed MRIs by utilizing the end-to-end DL network. Seitzer et al.[28] introduced a CS-based hybrid DL method that uses a visual refinement component as a learning objective on top of an MSE loss-based reconstruction network on the MRIs. However, none of the methods explore CS in X-ray imaging followed by pneumonia detection so as to serve the remote end analysis. Lu et al.[29] proposed a wireless DL-based CS reconstruction network (WDLReconNet) to address the adverse impact like channel noise and fading in wireless transmission. The DL-based approaches have shown lower computation complexity compared to the conventional CS reconstruction algorithms. In Reference 17, a DL framework is suggested by this research group for classifying pneumonia-affected X-ray images reconstructed from their subsample CS measurements. However, in contrast to the work in Reference 17, the present method uses a convolutional encoder to extract the useful features from the CS measurements itself and is then used for classification. The method also allows the reconstruction of the image at full scale. In other words, while pneumonia detection is performed on CS reconstructed images in Reference 17, the present work does the same job on CS measurements, facilitating the accurate diagnosis and computational benefit over Reference 17. DL network detects pneumonia on the CS measurements affected by the channel impairments at far-end communications.

2.2 | Scope and contributions of present work

A summary on the related works to highlight the present status of the present research problems is presented in Table 1. The literature review highlights a good number of works for pneumonia detection on chest X-ray images and CS image reconstruction as a separate research problem. Furthermore, pneumonia detection as a remote end solution is also not addressed much in these works. An accurate pneumonia detection algorithm applied directly on the CS measurements is useful in developing an application-specific disease diagnosis system. The method provides the desired support for tele-healthcare services operating on a low-bandwidth transmission environment. It is desirable that the method would extract the

TABLE 1 Review of the related works

Sl. No.	Method year	Approach	Findings	Limitations
1	Rajpurkar et al.[9] 2017	Applies transfer learning technique on DenseNet-121[21]	Identifies pneumonia directly from the chest X-rays	Very deep network and incapable of handling CS measurements
2	Kermany et al.[10] 2018	Adopting Inception-V3[22] through transfer learning for different diagnosis tasks	Generalizes the disease identification tasks from different medical images	Domain adaptation is compulsory and does not work on CS measurements
3	Jain et al.[11] 2020	Customized DL model utilizing CNN	Outperforms VGG-16,[23] ResNet-50,[24] and Inception-V3[22]	Fails to detect pneumonia from the CS measurements directly
4	Yu et al.[16] 2021	Graph-knowledge embedded CNN	A set of optimal features are obtained that improves pneumonia detection accuracy	Unable to extract features from the CS measurements
5	Mousavi et al.[26] 2017	Customized deep convolutional networks (DCNs)	Enables reconstruction at 100 times faster speed than the conventional CS methods	Direct matrix multiplication used in reconstruction steps may leads to aliasing artifacts
6	Yang et al.[27] 2017	DL model based on conditional generative adversarial network (GAN)	Enables faster reconstruction with a comparable reconstruction quality	Refinement strategy may lead to the elimination of significant information
7	Seitzer et al.[28] 2018	Compressed sensing (CS)-based hybrid DL method that uses a visual refinement component as a learning objective	Improves the training stability and produces high-quality reconstructions with large under-sampling factors	Performance often depends on the pretrained network utilized for segmentations
8	Lu et al.[29] 2019	Deep learning (DL)-based CS reconstruction network (WDLReconNet)	Capability to combat the adverse impact on the wireless channel like noise and fading effect	Use of feature enhancement layer may modify the actual values of features

most useful features for pneumonia detection from the subsampled measurements by mitigating the noise or other degradation caused during the transmission over the wireless channel. In addition to the pneumonia detection, the developed method should have the capability of providing the X-ray images such that radiologists or medical practitioners can validate the same. Towards this aim, this study extends the work presented in Reference 17 using a DL framework applied on CS measurements to provide a robust and low-cost pneumonia detection method. The method also enables X-ray image reconstruction at full scale for the patients located remotely. The overall contributions of the present work are listed as follows:

- A DL framework based on a customized CNN and fully connected neural network is designed and trained to detect pneumonia from the CS measurements of a chest X-ray image observed at remote locations. The novelty of the work is that high accuracy (96.48%) on pneumonia detection is achieved from subsample (30%) measurements at remote locations. The suggested solution leads to an energy- and bandwidth-efficient facility for tele-healthcare support.
- The DL framework utilizes an autoencoder to learn feature extraction from the CS measurements in an unsupervised way. The autoencoder provides the desired full-scale X-ray image as an output through the solution of an ill-posed inverse problem. The method leads to full-scale image reconstruction that can be used for subjective assessment by an expert medical person at far distance from the patients.
- The major issue in wireless transmission (radio mobile channel) is the adverse channel effect that degrades the reconstruction image quality as well as poor performance on pneumonia detection for the proposed method. To take into account, the proposed solution (network) combats the adverse effect of both additive noise and multiplicative degradation factors (Rayleigh fading effect) introduced by the transmission channel.

Since CS measurements are used directly on pneumonia detection, accuracy achieved is relatively high over the schemes that detect pneumonia on the reconstructed image.[17] The scheme also looks promising in future IoT-healthcare services due to its bandwidth and energy efficient transmission leading to an enhanced network lifetime of the IoT objects or nodes. Extensive simulation

results show that the proposed CS-based DL model can identify pneumonia with approximately 96.48% prediction accuracy from the X-ray images.

3 | MATERIALS AND METHODS

This section presents the proposed DL framework that detects pneumonia and reconstructs the X-ray images from CS measurements obtained through transmission over the wireless channel.

3.1 | CS measurement sensing and transmission

A signal $x \in \Re^N$ can be represented using a CS measurement vector $y \in \Re^M$ (where $M \ll N$) that is to be transmitted over a communication channel. The CS measurement vector can be expressed using the following equation[4]:

$$y = \Phi x + \eta, \tag{1}$$

where, $\Phi \in \Re^{M \times N}$ represents a linear sensing operator (measurement matrix) and $\eta \in \Re^N$ represents the noise introduced during the transmission.

In CS signal processing approach,[4,5] it is considered that the signal x has a sparse representation in some basis $\Psi = [\psi_1 | \psi_2 | ... | \psi_N]$ such that $x = \Psi s$ with $(K \ll N)$. Here, Ψ is an orthogonal basis and K is the number of nonzero coefficients present in the sparse signal s. Hence, Equation (1) can be written as

$$y = \Phi \Psi s + \eta = \mathbb{A} s + \eta, \tag{2}$$

where $\mathbb{A} = \Phi \Psi$, is the CS reconstruction matrix.

Now, considering the channel fading effect on the transmitted CS measurements, Equation (2) can be modified as

$$y = H \odot \mathbb{A} s + \eta, \tag{3}$$

where H is a random matrix representing the fading coefficients h_{ij}.

Among the various models of the radio mobile channel, Rayleigh distribution is considered in this work as it is reasonable to have no dominant propagation along a line of sight between the transmitter and the receiver. In the case of Rayleigh fading, the coefficients h_{ij} are independent and nonidentical random variables with $h_{ij} \sim \text{Rayleigh}(\nu_j)$ for $i = 0, 1, ..., M-1$ and $j = 0, 1, ..., N-1$. The $\text{Rayleigh}(\nu_j)$ fading model of channel gain represents a distribution with the probability density function (PDF) $f(x) = \frac{x}{\nu^2} e^{-\frac{x^2}{2\nu^2}}$, where x is a random variable with a nonzero positive value.

3.2 | Pneumonia detection and X-ray image reconstruction

The proposed DL framework accepts the CS measurements $y \in \Re^M$ as input and passes through a fully connected (FC) layer. The FC layer produces N number of neurons, which are then converted to $N_1 \times N_2 (= N)$ dimension as an estimation of the X-ray image, denoted by $\widetilde{x}$. The weight matrix of the FC layer is initialized with the values of $\mathbb{A}^T$ at the time of training of the network. The same sensing matrix that is utilized in the CS is also utilized for initializing the weight matrix to ensure the preservation of the original information.[26] However, the weight matrix gets updated through learning to reduce the under-sampling effect at the training time of the DL framework. A customized CNN, the encoder of the reconstruction model, learns to provide the most useful information in an unsupervised manner from $\widetilde{x}$. This is then used as a feature extractor shown in Figure 1. A multilayer neural network and a convolutional decoder network are utilized for performing the pneumonia detection and the X-ray image reconstruction process, respectively, as shown in Figure 1.

3.2.1 | The detection model

The proposed approach uses a deep neural network (DNN) to detect pneumonia from the CS measurements received through a communication channel as shown in Figure 1. In this approach, a copy of the X-ray image is first obtained by reshaping the response of an FC layer consisting of the same number of neurons as the actual X-ray image.

A DL model consisting of three convolutional and three FC layers is used as the detection network. The detection network considers the X-ray image obtained by reshaping the response of the first FC layer as an input. Convolutional layers are primarily responsible for extracting the most significant features from the input X-ray images. The extracted features are then used for the classification purpose by the FC layers. During training, the first convolutional layer learns to extract the low-level features such as the lines and the edges from the estimated X-ray images.[8] The second and the third convolutional layers learn to extract the features that are combinations of the lower-level features, such as features that comprise multiple lines and edges to express the shapes of the different objects

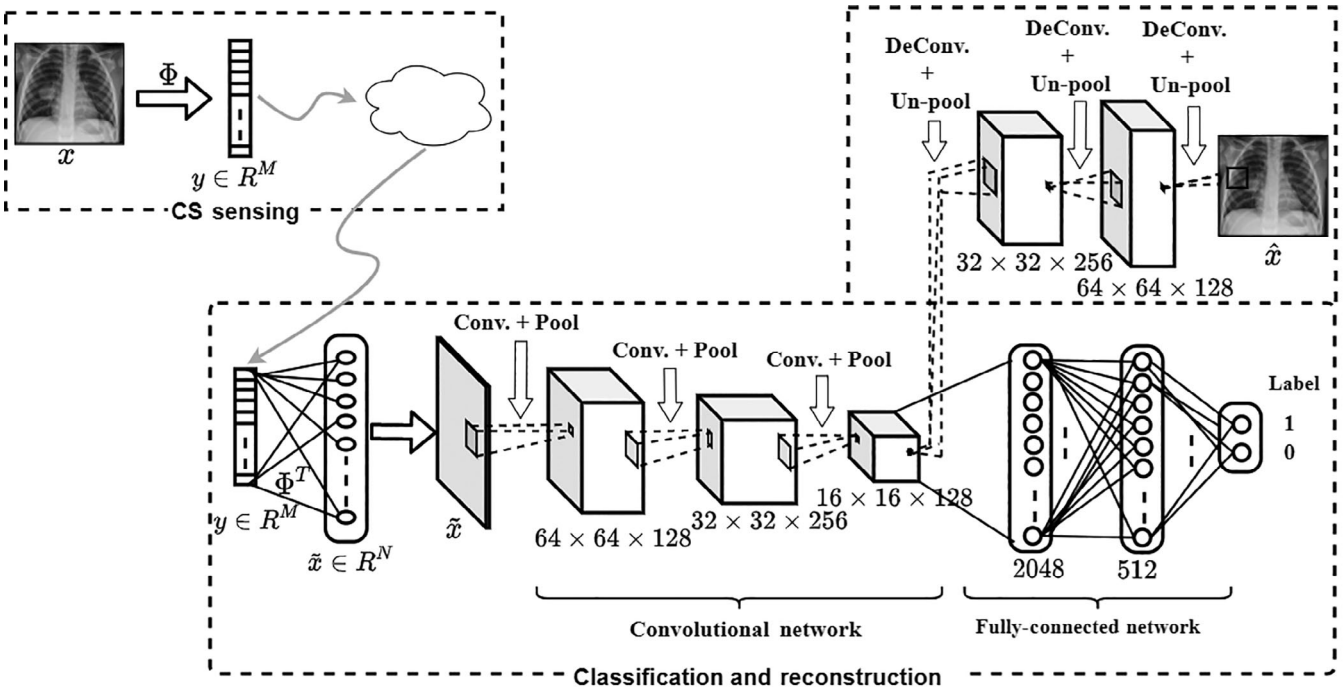

FIGURE 1 The proposed compressed sensing (CS)-based deep learning (DL) framework for pneumonia identification and reconstruction of the images

progressively.[8] The pooling layers used in the detection network enable reduction of the spatial dimension of the output (activation or features map) of the previous layer and provide a translation-invariant features map for the next layer. The output features map of a convolutional layer, followed by a pooling layer, can be obtained by the following equation:

$$h_k = \mathcal{S}(f_{lR}(W_k * \tilde{x} + b_k)), \tag{4}$$

where W_k, b_k, f_{lR}, and $\mathcal{S}$ are the set of the filters or the kernels, the biases used in the kth convolutional layer, nonlinear activation function, and sampling operator used in pooling layer, respectively.

The last three FC layers of the detection network are trained to identify, from the features extracted by the CNN, whether or not the chest X-ray is affected by pneumonia. Through training, each FC layer achieves a set of the optimal weights to be applied on the CNN extracted features towards making the final prediction. The output of any FC layer can be expressed mathematically as[23]

$$h_k^{\mathrm{FC}} = f_S\left(W_k^{\mathrm{FC}} h_k + b_k^{\mathrm{FC}}\right), \tag{5}$$

where W_k^{FC}, b_k^{FC}, and f_S represent the weights, the biases, and the activation function of the kth FC layer, respectively.

Finally, the output of the detection network can be defined to provide the decision as follows:

$$f(y)_c = \hat{p}(L_O = c|y),$$

where L_O denotes the respective output value and $c \in \{0,1\}$ is one of the two possibilities as output $\hat{p}$.

The learnable parameters, that is, the weights and the biases of the detection network are updated by minimizing the cross-entropy (negative log-likelihood) loss between the model's predicted output and the actual target output as shown in Equation (6).

$$L\left(f(y)_c; L_O\right) = -\sum_{c=0}^{1} L_O \log f(y)_c = -L_O \log f(y)_c. \tag{6}$$

Stochastic gradient descent (SGD) with the mini-batches[32] algorithm is used for optimizing the learnable network parameters during the training. The training steps of the detection network are summarized in Algorithm 1.

All the hidden layers of the detection network use leaky Rectified linear unit (ReLU) as activation function to introduce nonlinearity in the network. The use of leaky ReLu activation function ensures a nonzero gradient over its entire domain and is defined as

Algorithm 1

Training of the detection network

Input: Mini-batch of data $y_{i=1}^{B_N}$, Reconstruction matrix $\mathbb{A}$, Output label L_O, Step size α, Number of Epoch E_N
Initialize: The network parameters Θ
for $i=1$ **to** E_N **do**
  for $i=1$ **to** E_N **do**
    Predict $f(y)_c = \widehat{p}(L_O = c|y)$
  Compute Loss $L\left(f(y)_c; L_O\right) = -L_O \log f(y)_c$
  Update $\Theta \leftarrow \Theta - \frac{\delta}{\delta x}\left(L\left(f(y)_c; L_O\right)\right)$

$$f_{lR}(\text{input}) = \begin{cases} \text{input} & \text{if input} > 0 \\ 0.001*\text{input} & \text{otherwise} \end{cases}.$$

The final layer uses sigmoid activation function defined as follows:

$$f_S(\text{input}) = \frac{1}{1+e^{-\Theta^T * \text{input}}},$$

where Θ denotes the learnable parameters, that is, the weight matrices W and the bias vectors b.

3.2.2 | The image reconstruction model

Besides pneumonia detection, the proposed method keeps provisioning of the full-scale reconstruction of the X-ray image from its CS measurements received through the communication channel. The reconstructed X-ray image can be used by a domain expert to identify/verify the presence of pneumonia manually.

In CS, the image reconstruction is an ill-posed inverse problem that looks for an estimation $\hat{x}$ of the image. Successful reconstruction of the original X-ray image needs to minimize the following objective function[4]:

$$\hat{x} = \underset{x \in S_c}{\operatorname{argmin}} \|\Phi x - y\|_2^2 + \lambda \varphi(x), \tag{7}$$

where $x = \Psi s$, S_c, $\lambda > 0$, and φ represent the signal to be reconstructed, a convex set, a constant that trades off the weights in the objective function, and a regularization parameter, respectively.

The objective function, defined in Equation (7), can be equivalently learnt by a convolutional autoencoder (CAE) as shown in Figure 1. The CNN that is utilized as the features extractor in the detection network is also considered as the encoder of the CAE. The decoder is implemented by another CNN consisting of three convolutional layers as shown in Figure 1. The compressed features extracted by the encoder are used by the decoder to reconstruct the desired X-ray image. The decoder uses the same number of filters along with an up-sampling (unpooling) operator in the reverse order.

In each iteration, during training, the reconstructed image is updated using a quasi-projection operator $Q(\hat{x}; W)$ parametrized by a set of weights W of the CAE through gradient descent[26]:

$$\hat{x}^n = Q\left(\hat{x}^{n+1} - \alpha \nabla C\left(\hat{x}^{n-1}\right)\right), \tag{8}$$

where the Q is projected onto the set of artifact-free X-ray images, n is the number of iterations, α is the step size, and $C(\hat{x}^n)$ is the cost function. To establish the stability in the reconstruction model, this work enforces restricted isometry property (RIP)[33] via minimizing the reconstruction loss during training. The loss function is used as follows:

$$C\left(\hat{x}^{(n)}\right) = \mathbb{E}_{x^n, \hat{x}^n}\left[\left(\|\Phi(x^n - \hat{x}^n)\|_2 - \|x^n - \hat{x}^n\|_2\right)^2\right], \tag{9}$$

$\mathbb{E}(.)$ and Φ represent the expectation and the random measurement matrix, respectively. The training steps of the reconstruction network are summarized in Algorithm 2.

Algorithm 2

Training of the reconstruction network

Input: Mini-batch of data $y_{i=1}^{B_N}$, Reconstruction matrix $\mathbb{A}$, Step size α, Number of Epoch E_N
Initialize: The network parameters Θ
for $i=1$ **to** E_N **do**
  for $i=1$ **to** B_N **do**
    Optimize $\hat{x}_i \leftarrow \hat{x}_i - \frac{\delta}{\delta x}\mathbb{E}_\Theta(x_i, \hat{x}_i)$
  Compute Loss $C\left(\hat{x}^{(n)}\right) = \mathbb{E}_{x^n, \hat{x}^n}$
    $\left[\left(\|F(x^n - \hat{x}^n)\|_2 - \|x^n - \hat{x}^n\|_2\right)^2\right]$
  Update $\Theta \leftarrow \Theta - \frac{\delta}{\delta x}\left(C\left(\hat{x}^{(n)}\right)\right)$

3.3 | Description of the network

This subsection describes the layers and the kernels of the proposed pneumonia detection and reconstruction framework in details.

3.3.1 | Features extraction

Input: Measurement vector, $y \in \Re^M$.

FC-0: An FC layer with $N(\text{width} \times \text{height}) \times N_{ch}$ (number of channels) neurons to obtain the proxy $\widetilde{x}$ of the X-ray image x.

Conv-1: A convolutional layer consisting of 128 kernels of dimension 5×5 is applied with a stride of 1 and padding of 1.

MaxPool-1: A pooling layer of size 2×2 and stride 2.

Conv-2: The next convolutional layer consists of 256 kernels of size 3×3 applied with a stride of 1 and padding of 1.

MaxPool-2: The second pooling layer, following the convolutional layer, uses the kernels of size 2×2 and stride 2.

Conv-3: The third convolutional layer consists of 128 kernels of size 3×3 applied with a stride of 1 and padding of 1.

MaxPool-3: The next layer performs the pooling operation using 2×2 kernels and a stride of 2.

By utilizing the three convolutional layers, the required hierarchical features (i.e., from edges to small objects) can be extracted to achieve the desired accuracy with generalization. Increasing the number of layers often increases the accuracy with an incremental value. However, the possibilities of the data overfitting to the model are also increased. On the other hand, consideration of the less number of layers often fails to capture the underlying data pattern to meet the objective.

3.3.2 | Classifying X-ray images

FC-1: An FC layer with 2048 neurons follows the convolutional layers.

FC-2: Another FC layer is constructed with 512 neurons.

FC-3: Final FC layer having two neurons to assign a label as output.

In the case of the FC neural network, an increase in the number of layers or neurons increases the complexity of the model, which may lead to the overfitting problem like the deep CNN. In addition, the computational power requirements for the training of the complex network are also increased significantly. On the flip side, a sallow neural network fails to generalize the accuracy of the model. Considering all the aspects, a three-layered FC network is chosen for the classification purpose.

3.3.3 | Full-scale image reconstruction

The reconstruction network is constructed with the deconvolutional and unpooling layers having the same number of kernels as the features extraction network, however, are arranged in the reverse order as described below.

De-Conv-1: A deconvolutional layer that consists of total 256 kernels of size 3×3 used with a stride of 1 and padding of 1.

Un-Pool-1: An un-pooling layer following the deconvolutional layer consisting of 2×2 sized kernels and stride 2.

De-Conv-2: The second deconvolutional layer consists of 128 kernels of size 3×3 used with stride of 1 and padding of 1.

Un-Pool-2: Another un-pooling layer with a kernel of 2×2 is applied with a stride of 2.

De-Conv-3: The final deconvolutional layer consists of N_{ch} kernels of size 5×5 used with a stride of 1 and a padding of 1.

Un-Pool-3: An un-pool layer is used to obtain the desired sized X-ray image using kernels of 2×2 and a stride of 2.

3.4 | Dataset preparation for training

This work uses the dataset obtained from Kaggle,[34] which consists of total 5856 X-ray images (normal and pneumonia) divided into training, validation, and test sets with 5216, 16, and 624 images, respectively. The dataset is then increased by an amount of about 20% using additive random Gaussian noise (with 0 mean) as well as multiplicative Rayleigh fading (with varying channel SNR from 10 to 20 dB). After performing the data augmentation, the total number of X-ray images in the dataset is increased to 7027 (normal—1900 and pneumonia—5127). This work rearranges all the normal and pneumonia images and divides into an approximately 70% for the training, 25% for the validation, and 5% for the test purpose. All the X-ray images are resized into 128×128 to reduce the required computational burden during training. The discrete cosine transform (DCT) for an one-dimensional sequence $\{x_0, x_1, ..., x_{N-1}\}$, as shown in Equation (10), is used as sparsifying basis for the images.

$$x_k = \sum_{n=0}^{N-1} x_n \cos\left[\frac{\pi}{N}\left(n + \frac{1}{2}\right)k\right], \tag{10}$$

where $k = 0, 1, 2, ..., N-1$.

Here, x_n and X_K represent the spatial domain data and the DCT coefficients, respectively.

To obtain the CS measurement (observations), an independent and identically distributed (IID) Gaussian matrix of $\Re^{M \times N}$ is used as the sensing matrix Φ for all the X-ray images to prepare the required dataset.

4 | SIMULATION RESULTS

This section illustrates the performance of the proposed approach in terms of prediction accuracy of pneumonia. The performance of the reconstruction network is also evaluated through the quality of the reconstructed X-ray images in terms of quantitative assessment measured by peak-signal-to-noise ratio (PSNR) and mean Structural SIMilarity (SSIM). The training and the testing of the DL network of the present work are carried out in Google's online cloud support tool known as Colaboratory (Colab). The "runtime type" and "hardware accelerator" in the Colab are chosen as "Python3" and "GPU," respectively. The KERAS libraries and packages with TensorFlow 2.0 as backend are used as the development environment.

4.1 | Pneumonia detection performance

Figure 2 shows the plot of the pneumonia detection accuracy for both the training and the validation data obtained in each epoch. The plot describes the performance of the learning process where the training and the validation accuracy reach 96.41% and 95.58%, respectively, after the completion of 400 epochs. This study also presents the variation on the loss evaluated using Equation (6) in every epoch as shown in Figure 3. As expected, both the training and the validation loss go on reducing with the progress of the learning process. This work uses the dropout regularization for all the FC layers and batch normalization (BN) for the first FC hidden layer to prevent the overfitting problem.

Performance of the trained pneumonia detection model is evaluated using the test dataset and is compared with the existing methods such as Inception-TL,[10] Customized CNN,[11] ChexNet,[9] and CGNet,[16] in terms of the prediction accuracy as reported in Table 2. In this experiment, the test dataset also includes the measurements affected by channel Rayleigh fading and additive Gaussian noise as discussed in Section 3.4. Since the methods presented in References 9–11,16 do not work on CS measurements, the experiment uses the same CS reconstructed X-ray images from the same number of measurements as used in the proposed method, in order to make a fair comparison. This experiment considers different numbers of CS measurements; however, numerical values of the prediction accuracy for 20% and 30% measurements are tabulated. Relatively high image quality achieved even at low measurements highlights the merit of the proposed CS reconstruction network through this learning-based method. The comparative study in terms of the graphical representation for the different percentages (%) of the input measurements is shown in Figure 4. As expected, the prediction accuracy is improved with the increasing sampling ratio (measurements). The prediction accuracy of the proposed method (PM) outperforms the existing Inception-TL,[10] Customized CNN,[11] ChexNet,[9] and CGNet[16] methods as shown in Figure 4. It is worth mentioning that the use of 30% measurements implies a savings in bandwidth by 70% w.r.t. its full resolution. The transmission of the less number of measurements not only causes savings in bandwidth but also highlights low energy required for the data transmission. Actual energy savings analysis may be explored as future work.

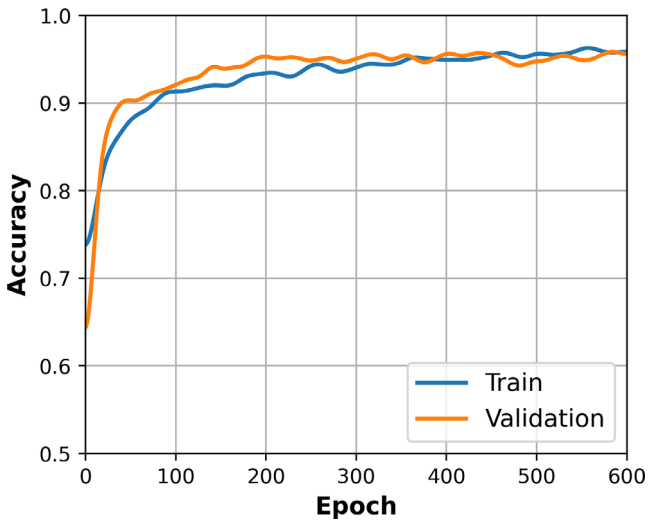

FIGURE 2 Performance evaluation of detection network: prediction accuracy versus epoch

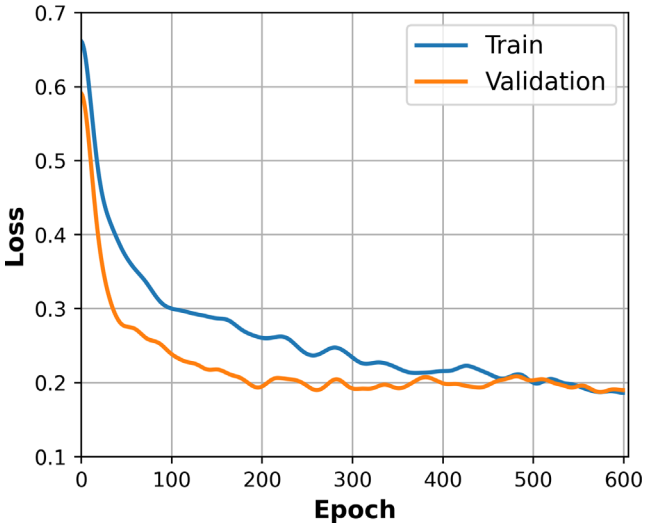

FIGURE 3 Performance evaluation of detection network: loss versus epoch

TABLE 2 Performance comparison on prediction accuracy

	M (%)	Inception-TL[10]	Customized CNN[11]	ChexNet[9]	CGNet[16]	PM
Prediction accuracy (%)	20	89.61	91.00	93.50	94.13	**95.22**
Prediction accuracy (%)	30	91.16	92.83	95.28	95.60	**96.48**

Note: The significance of bold values represent the best results.

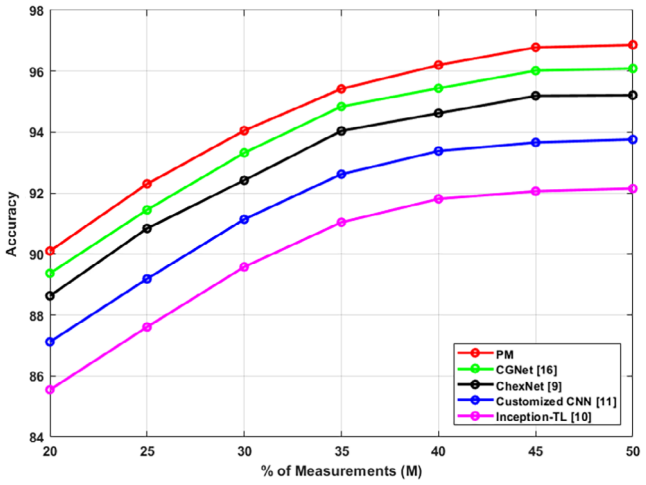

FIGURE 4 Performance evaluation: accuracy versus (%) of measurement

4.2 | Performance of CS image reconstruction

This section presents the performance of the reconstruction network in terms of the perceptual quality of the X-ray images. A comparative study of the proposed method over the existing methods such as DL-guided CS,[28] DCNs,[26] DAGAN,[27] and DLNet[29] is also performed and reported in terms of the quantitative as well as qualitative measures. To have a fair comparison, the proposed method is simulated considering the transmission channels as ideal; that is, noise-free CS measurements are used as input to the network. The corresponding reconstructed X-ray images are presented in Figure 5. The results show that Figure 5E,J, obtained using the proposed approach, achieve superior reconstruction quality while compared with Figure 5A–D, F–I. The reconstruction quality is also assessed in terms of the PSNR and SSIM values to quantify the quality of the proposed method along with the other methods[26–29] as reported in Table 3. The PSNR and SSIM values are obtained by averaging 50 independent run results considering 20% and 30% CS measurements. As expected, the proposed method achieves the maximum PSNR (30) and SSIM (0.85) values when 30% measurements are used compared to the existing methods.[26–29]

Performance of the proposed DL framework is also studied in the presence of the channel Rayleigh fading effect considering low channel signal-to-noise ratio (CSNR). The objective of this study is to compare the X-ray image quality reconstructed from the CS measurements obtained through a channel with adding some adverse effects. Reconstructed X-ray images using the DL-guided CS,[28] DCNs,[26] DAGAN,[27] DLNet,[29] and the proposed DL framework are shown in Figure 6 when considering the CSNR value of 15 dB. This comparative study utilizes 20% and 30% CS measurements for all the methods. The reconstructed X-ray images presented in Figure 6E,J show the better perceptual quality compared to Figure 6A–D,F–I, respectively. This study also reports a quantitative assessment on the reconstruction quality of the images obtained through the different methods as reported in Table 4. The PSNR and SSIM values are considered for the quantitative assessment result comparison. Reported values are obtained by averaging 50 independent run results. As expected, the proposed method achieves the maximum PSNR and SSIM values compared to the DL-guided CS,[28] DCNs,[26] DAGAN,[27] and DLNet[29] methods.

This study shows that the proposed method enables the detection of pneumonia as well as reconstruction of the desired X-ray image from the under-sampled CS measurements. The CS framework allows reduction in the number of the observed samples that in turn also reduces the requirement of the channel bandwidth by reducing the bit rate (i.e., number of bits to be transmitted per second). Hence, the proposed method shows its effectiveness in real-time application over a band-limited channel by reducing the transmission burden. The experimental results, shown in Tables 3 and 4, validate the fact.

5 | DISCUSSION

In the proposed method, the measurements are projected through the Φ^T-weighted FC layer as the first hidden layer with total N number of neurons. Here, N is the number of pixels present in the full-scale X-ray image. The method offers universality in choosing any sampling ratio (or % of measurements) satisfying RIP as the FC layer aims at providing a vector of the required

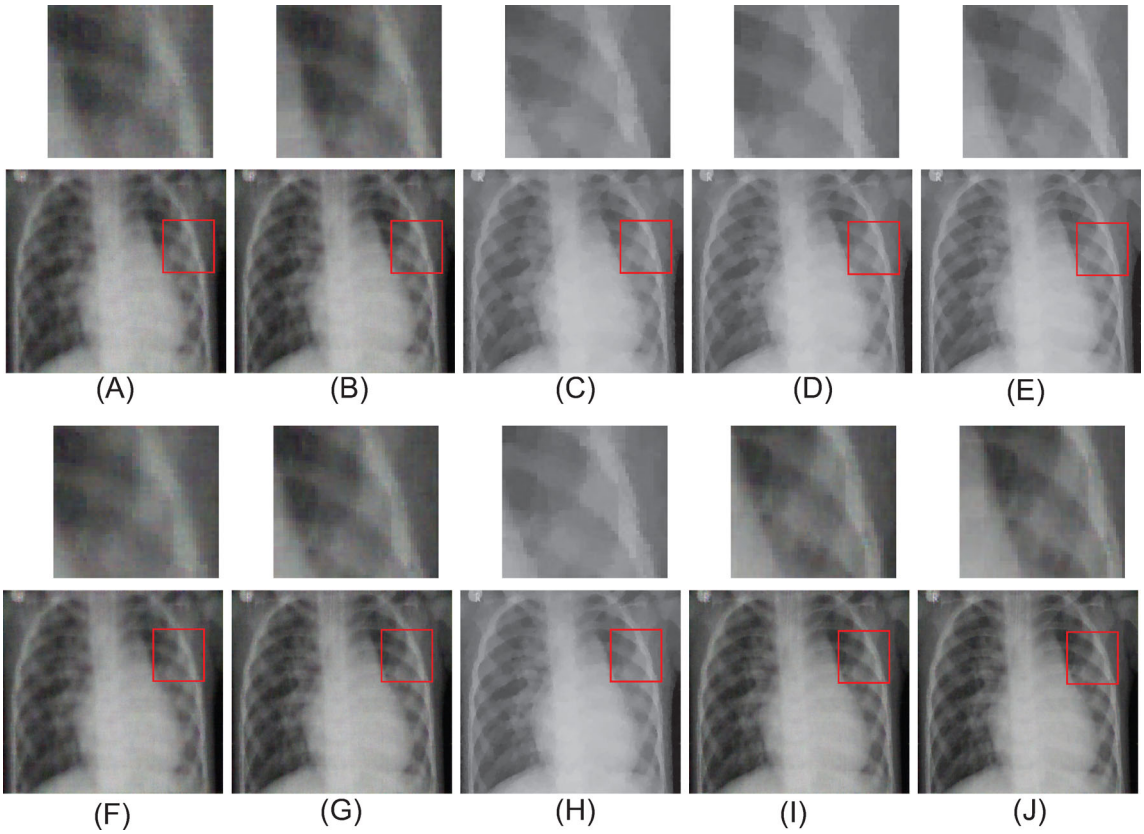

FIGURE 5 Performance comparison: (A–E) and (F–J) are the reconstructed X-ray images using DL-guided CS,[28] DCNs,[26] DAGAN,[27] DLNet,[29] and the proposed method while 20% and 30% measurements are used. The red marked portions are shown (with ×4 magnification) in above each of the images

TABLE 3 Performance comparison of reconstructed X-ray images using different methods at sensing end

Metric used	M (%)	DL-CS[28]	DCNs[26]	DAGAN[27]	DLNet[29]	PM
PSNR (dB)	20	25.76	26.88	28.52	28.70	**29.04**
SSIM		0.77	0.79	0.81	0.81	**0.82**
PSNR (dB)	30	27.90	28.50	29.18	29.21	**30.85**
SSIM		0.80	0.81	0.83	0.83	**0.85**

Note: The significance of bold values represent the best results.

dimension for the DL network. The output of the first hidden layer is then reshaped as $N_1 \times N_2$ dimension to be fed to the convolutional network as shown in Figure 1. The N_1 and N_2 are the number of the rows and the columns (i.e., $N = N_1 \times N_2$) present in the X-ray image, respectively. By applying Φ^T operator on the measurements and after reshaping, a noisy version of the actual X-ray image is obtained. As mentioned in Section 3.4, a number of noisy samples are used to train the network to extract the most useful information by a convolutional encoder and use them as per requirement by the subsequent layers.

This work performs BN to ensure no activation passes too high or too low throughout the network before feeding the inputs to the convolutional layer. The use of BN layer adds regularization effect to prevent the model to be overfitted by the training data.[35] This work uses kernels of size 5×5 with a stride of 1 for all the convolutional layers. All the hidden layers use the leaky ReLu activation function to ensure that no negative activation disappears completely. The pooling layers perform 50% down-sampling (in each direction) using kernels of size 2×2 with a stride of 2.

The values for the hyperparameters used in this work are mentioned in Table 5. A good combination of the hyperparameter values can improve the model's performance significantly. A computationally expensive technique such as Random search[36] and Bayesian optimization[37] can be utilized to obtain the set of optimal values for the hyperparameters. However, this work

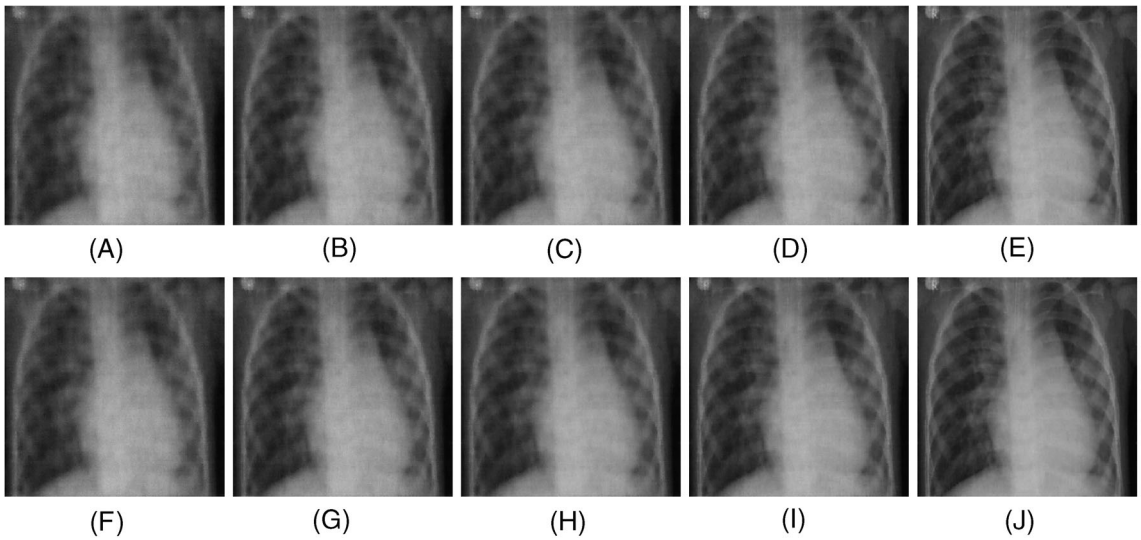

FIGURE 6 Performance comparison: (A–E) and (F–J) are the reconstructed X-ray images using DL-guided CS,[28] DCNs,[26] DAGAN,[27] DLNet,[29] and the proposed method while 20% and 30% measurements considering 15 dB CSNR are used

Metric used	M (%)	DL-CS[28]	DCNs[26]	DAGAN[27]	DLNet[29]	PM
PSNR (dB)	20	21.24	22.30	24.33	24.70	**25.47**
SSIM		0.71	0.72	0.75	0.75	**0.77**
PSNR (dB)	30	22.45	23.54	24.92	25.09	**26.22**
SSIM		0.74	0.75	0.77	0.78	**0.80**

TABLE 4 Performance comparison of reconstructed X-ray images using different methods and % of measurements while CSNR= 15 dB is considered

Note: The significance of bold values represent the best results.

TABLE 5 Hyperparameters used in the training

Hyperparameter	Value
Batch size	32
Learning rate (initial), α	0.021
Momentum	0.6
Dropout rate	0.4

chooses the values of the hyperparameters through manual tuning to avoid the heavy computational requirement. It is worth mentioning that considering too small value for the learning rate slows down the convergence. On the other hand, if the value of the learning rate is too high, the desired convergence never be achieved. A larger batch size often helps to choose a larger learning rate. However, a larger batch size also demands a high computational requirement. Considering all the points, a moderate learning rate is used to train the network. The use of momentum with the appropriate learning rate helps the model to accelerate the learning process and offers a stable accuracy. However, a very large value for the momentum may overshoot the global minima. Dropout adds regularization to the learning process and addresses the overfitting problem. This work uses the value for the dropout such that the important features are preserved while the overfitting problem is also reduced.

During the training of the network, the model learns to extract the preserved information in $\tilde{x}$. The first layer of the convolutional encoder finds the simple features like the edges, and the subsequent convolutional layers gradually learn to find the shapes of the complex objects present in $\tilde{x}$. The prime objective of the pooling layers, used in the encoder, is to reduce the spatial dimension of the input features. All the compressed features extracted by the convolutional encoder are then combined to assign the desired label to the input by a detection subnetwork consisting of three FC layers. The final layer of the detection network consists of only two neurons to indicate whether pneumonia is present or not.

A convolutional decoder network is used as a reconstruction submodel to be trained to provide the desired reconstructed X-ray images from $\tilde{x}$. The reconstruction subnetwork consists of deconvolutional and unpooling layers alternately to provide the full-scale denoised X-ray image from the compressed features extracted by the

encoder. The deconvolutional layers are responsible to reconstruct the original image from the compressed features, while the unpooling layers progressively increase the spatial dimension to the actual size. The main objective of the training is to make both the encoder and the decoder network together to be capable of denoising the input noisy version of the X-ray image obtained by inverse transform of the CS measurements. As the ground truth X-ray images are used in the training, to back-propagate the error for the updating of the learnable parameters, the trained reconstruction network is able to provide the X-ray images with the desired quality.

It is worth mentioning that both the time and space complexity of a DNN model are closely related to the number of parameters of the model. The computational complexity increases with the increasing number of parameters and the size of the input. In this context, the proposed DL model has the number of learnable parameters present in the first FC layer, feature extraction network, classification network, and reconstruction network are 48 M, 600 K, 68 M, and 600 K, respectively. In total, the whole DL framework consists of 117.2 M parameters. Typically, a complex DL network performing an image recognition task can have 50 M to 138 M parameters, depending upon the size of the input image.[38] However, the proposed network serves both the recognition as well as reconstruction tasks with the help of the lesser number of parameters compared to the network presented in Reference 23. In real-time applications, hardware accelerators (graphics processing unit) are usually used for inferring the DL models to optimize the execution time.

The proposed DL framework achieves the paramount objective of this work, that is, reduction on the required channel bandwidth for the far-end pneumonia detection as well as the reconstruction of the X-ray image at the receiving end from subsample measurements. The proposed method detects pneumonia with more than 96% accuracy from only 30% CS measurements obtained at the receiving end. The method also provides the X-ray image with PSNR ∼26.22 dB and SSIM ∼0.80 for the same CS measurements at the receiving end.

6 | CONCLUSIONS AND FUTURE WORKS

This article develops a DL network that enables direct detection of pneumonia on the CS measurements of any chest X-ray image obtained through a far-end communication channel. The DL model also provides the full-scale X-ray image reconstructed from the CS measurements. The CNN architecture consists of three pairs of the convolutional and the pooling layers to extract the significant features in a compressed form. A dense subnetwork, consisting of three FC layers, is then used to detect the presence of pneumonia. Another subnetwork, consisting of three pairs of deconvolutional and unpooling layers, is used to provide the full-scale X-ray image. The study shows that the use of the DL approach enables pneumonia detection with high accuracy when applied in CS-based signal processing framework, compared to the conventional methods. The simulation results show that the proposed approach offers 96.48% prediction accuracy when 30% CS measurements are used, leading to the savings in 70% bandwidth. The savings in energy computation for CS data transmission can be analyzed as a future work.

The proposed approach can also be explored for detecting COVID-19 pneumonia using TL technique. The method can also be further extended as a generalized automatic computerized system to assist medical professionals by localizing the region of interest (ROI), such as brain tumor, cancerous cell, kidney, and gallbladder stone.

DATA AVAILABILITY STATEMENT

Data sharing is not applicable to this article as no new data were created or analyzed in this study.

ORCID

Santi P. Maity https://orcid.org/0000-0002-1075-3829
Mrinal Mandal https://orcid.org/0000-0002-0680-5876

REFERENCES

1. Bates JH, Campbell GD, Barton AL, et al. Microbial etiology of acute pneumonia in hospitalized patients. *Chest*. 1992;101(4):1005-1012.
2. U.S. Department of Health Human Services. Accessed November 27, 2019. https://www.cdc.gov/features/pneumonia/index.html
3. Kar SS, Maity SP. Gradation of diabetic retinopathy on reconstructed image using compressed sensing. *IET Image Process*. 2018;12(11):1956-1963.
4. Donoho DL. Compressed sensing. *IEEE Trans Inf Theory*. 2006;52(4):1289-1306.
5. Baraniuk RG. Compressive sensing. *IEEE Signal Process Mag*. 2007;24(4):118-120.
6. Graff CG, Sidky EY. Compressive sensing in medical imaging. *Appl Opt*. 2015;54(8):C23-C44.
7. Obrzut S, Nguyen B, Sung A, Song B. Compressed sensing approaches to low-radiation CT reconstruction. *J Nucl Med*. 2016;57(supplement 2):1283-1283.
8. LeCun Y, Bengio Y, Hinton G. Deep learning. *Nature*. 2015;521(7553):436.
9. Rajpurkar P, Irvin J, Zhu K, et al. Chexnet: radiologist-level pneumonia detection on chest x-rays with deep learning. ArXiv Preprint arXiv:171105225, 2017.

10. Kermany DS, Goldbaum M, Cai W, et al. Identifying medical diagnoses and treatable diseases by image-based deep learning. *Cell*. 2018;172(5):1122-1131.
11. Jain R, Nagrath P, Kataria G, Kaushik VS, Hemanth DJ. Pneumonia detection in chest X-ray images using convolutional neural networks and transfer learning. *Measurement*. 2020;165:108046.
12. Toğçar M, Ergen B, Cömert Z, Özyurt F. A deep feature learning model for pneumonia detection applying a combination of mRMR feature selection and machine learning models. *Innov Res BioMed Eng*. 2020;41(4):212-222.
13. Liang G, Zheng L. A transfer learning method with deep residual network for pediatric pneumonia diagnosis. *Comput Methods Prog Biomed*. 2020;187:104964.
14. Yee SLK, Raymond WJK. Pneumonia diagnosis using chest X-ray images and machine learning. Paper presented at: Proceedings of the 10th International Conference on Biomedical Engineering and Technology; 2020, pp. 101–105.
15. Chouhan V, Singh SK, Khamparia A, et al. A novel transfer learning based approach for pneumonia detection in chest X-ray images. *Appl Sci*. 2020;10(2):559.
16. Yu X, Wang SH, Zhang YD. CGNet: a graph-knowledge embedded convolutional neural network for detection of pneumonia. *Inf Process Manag*. 2021;58(1):102411.
17. Islam SR, Maity SP, Ray AK, Mandal M. Automatic detection of pneumonia on compressed sensing images using deep learning. Paper presented at: Proceedings of the IEEE Canadian Conference of Electrical and Computer Engineering (CCECE) IEEE; 2019, pp. 1–4.
18. Fiszman M, Chapman WW, Evans SR, Haug PJ. Automatic identification of pneumonia related concepts on chest x-ray reports. Paper presented at: Proceedings of the American Medical Informatics Association Symposium AMIA, 1999, p. 67.
19. Chapman WW, Fizman M, Chapman BE, Haug PJ. A comparison of classification algorithms to automatically identify chest X-ray reports that support pneumonia. *J Biomed Inform*. 2001;34(1):4-14.
20. Mendonca EA, Haas J, Shagina L, Larson E, Friedman C. Extracting information on pneumonia in infants using natural language processing of radiology reports. *J Biomed Iinform*. 2005;38(4):314-321.
21. Huang G, Liu Z, Van Der Maaten L, Weinberger KQ. Densely connected convolutional networks. Paper presented at: Proceedings of the IEEE Conference on Computer Vision and Pattern Recognition (CVPR); 2017, pp. 4700–4708.
22. Szegedy C, Vanhoucke V, Ioffe S, Shlens J, Wojna Z. Rethinking the inception architecture for computer vision. Paper presented at: Proceedings of the IEEE Conference on Computer Vision and Pattern Recognition (CVPR); 2016, pp. 2818–2826.
23. Simonyan K, Zisserman A. Very deep convolutional networks for large-scale image recognition. arXiv Preprint arXiv: 14091556; 2014.
24. He K, Zhang X, Ren S, Sun J. Deep residual learning for image recognition. Paper presented at: Proceedings of the IEEE Conference on Computer Vision and Pattern Recognition (CVPR); 2016, pp. 770–778.
25. Krizhevsky A, Sutskever I, Hinton GE. Imagenet classification with deep convolutional neural networks. *Adv Neural Inf Proces Syst*. 2012;25:1097-1105.
26. Mousavi A, Baraniuk RG. Learning to invert: signal recovery via deep convolutional networks. Paper presented at: Proceedings of the IEEE International Conference on Acoustics, Speech and Signal Processing (ICASSP) IEEE; 2017, pp. 2272–2276.
27. Yang G, Yu S, Dong H, et al. DAGAN: deep de-aliasing generative adversarial networks for fast compressed sensing MRI reconstruction. *IEEE Trans Med Imaging*. 2017;37(6):1310-1321.
28. Seitzer M, Yang G, Schlemper J, et al. Adversarial and perceptual refinement for compressed sensing MRI reconstruction. Paper presented at: Proceedings of the International Conference on Medical Image Computing and Computer-Assisted Intervention Springer; 2018, pp. 232–240.
29. Lu H, Bo L. WDLReconNet: compressive sensing reconstruction with deep learning over wireless fading channels. *IEEE Access*. 2019;7:24440–24451.
30. Metzler CA, Maleki A, Baraniuk RG. From denoising to compressed sensing. *IEEE Trans Inf Theory*. 2016;62(9):5117-5144.
31. Gregor K, LeCun Y. Learning fast approximations of sparse coding. Paper presented at: Proceedings of the 27th International Conference on Machine Learning (ICML) Omnipress; 2010, pp. 399–406.
32. Rumelhart DE, Hinton GE, Williams RJ, et al. Learning representations by back-propagating errors. *Cognit Model*. 1988;5(3):1.
33. Baraniuk R, Davenport M, DeVore R, Wakin M. A simple proof of the restricted isometry property for random matrices. *Constr Approx*. 2008;28(3):253-263.
34. Chest X-ray images (pneumonia). Accessed August 16, 2019. https://www.kaggle.com/paultimothymooney/chest-xray-pneumonia
35. Ioffe S, Szegedy C. Batch normalization: accelerating deep network training by reducing internal covariate shift. Paper presented at: Proceedings of the International Conference on Machine Learning (ICML) PMLR; 2015, pp. 448–456.
36. Bergstra J, Bengio Y. Random search for hyper-parameter optimization. *J Mach Learn Res*. 2012;13(2):281-305.
37. Snoek J, Larochelle H, Adams RP. Practical bayesian optimization of machine learning algorithms. ArXiv Preprint ArXiv: 12062944 2012.
38. Khan A, Sohail A, Zahoora U, Qureshi AS. A survey of the recent architectures of deep convolutional neural networks. *Artif Intell Rev*. 2020;53(8):5455-5516.

How to cite this article: Islam SR, Maity SP, Ray AK, Mandal M. Deep learning on compressed sensing measurements in pneumonia detection. *Int J Imaging Syst Technol*. 2022;32(1):41-54. doi: 10.1002/ima.22651